https://doi.org/10.5194/egusphere-2026-4773
Preprint. Discussion started: 8 September 2026

Improving bottom-up ammonia emission estimations in Guangdong combining ammonia measurements from a ground-based network and FY-4B satellite and GCHP model

Lingze Meng[1,2], Ni Lu[1], Yixin Guo[1], Ziru Lan[1], Zhao-Cheng Zeng[3], Zichong Chen[1,4], Yuanhong Zhao[5,6], Zhuangmin Zhong[2,7], Tao Zhang[2,7], Duohong Chen[2,7], Xuejun Liu[8], Lin Zhang[9], Junyu Zheng[10]

[1] Earth, Ocean and Atmospheric Sciences Thrust, Function Hub, Hong Kong University of Science & Technology (Guangzhou), Guangzhou 511442, China

[2] Key Laboratory of Regional Air Quality Monitoring, Ministry of Ecology and Environment, Guangzhou 510060, China

[3] School of Earth and Space Sciences, Peking University, Beijing 100871, China

[4] Thrust of Carbon Neutrality and Climate Change, Society Hub, Hong Kong University of Science & Technology (Guangzhou), Guangzhou 511442, China

[5] State Key Laboratory of Physical Oceanography, Ocean University of China, Qingdao 266100, China

[6] College of Oceanic and Atmospheric Sciences, Ocean University of China, Qingdao, 266100, China

[7] Guangdong Ecological and Environmental Monitoring Center, Guangzhou 510060, China

[8] State Key Laboratory of Nutrient Use and Management, College of Resources and Environmental Sciences, National Academy of Agriculture Green Development, National Observation and Research Station of Agriculture Green Development (Quzhou, Hebei), China Agricultural University, Beijing 100193, China

[9] Laboratory for Climate and Ocean-Atmosphere Studies, Department of Atmospheric and Oceanic Sciences, School of Physics, Peking University, Beijing 100871, People's Republic of China

[10] Sustainable Energy and Environment Thrust, Function Hub, Hong Kong University of Science & Technology (Guangzhou), Guangzhou 511442, China

Correspondence to: Yixin Guo (yixinguo@hkust-gz.edu.cn)

Abstract

Accurate ammonia (NH_3) emission inventories are critical for $PM_{2.5}$ mitigation, yet bottom-up estimates remain uncertain, particularly for sector-resolved estimates in humid subtropical regions such as Guangdong, where urban-industrial emissions in the Pearl River Delta (PRD) coexist with dispersed agricultural sources in surrounding non-PRD areas. Here we integrate a ground-based NH_3 network, Fengyun-4B (FY-4B) geostationary NH_3 retrievals, a localized 3 km × 3 km prior inventory, and stretched-grid GEOS-Chem High Performance (GCHP) simulations at 0.2° × 0.2° resolution to inversely constrain monthly agricultural and non-agricultural NH_3 emissions in the PRD and non-PRD Guangdong in 2023. The posterior simulation improved agreement with observations, reducing NRMSE from 55.3% to 48.4% and changing NMB from -9.0% to 4.6%, with further support from independent NH_3, NH_4^+, and

https://doi.org/10.5194/egusphere-2026-4773
Preprint. Discussion started: 8 September 2026

deposition measurements. Provincial anthropogenic NH_3 emissions decreased from 477.6 to 441.5 kt yr^{-1}: agricultural emissions declined from 437.2 to 362.5 kt yr^{-1}, mainly through warm-season reductions in non-PRD areas, whereas non-agricultural emissions increased from 40.4 to 79.0 kt yr^{-1}, especially during the cool season. Hypothetically removing agricultural (non-agricultural) NH_3 emissions in Guangdong provided provincial $PM_{2.5}$ reductions of 3.7 ± 1.5 (0.7 ± 0.4) μg m^{-3} and avoided premature deaths of 3251 (1064), highlighting the need to combine dispersed agricultural source controls and targeted non-agricultural source controls over populated PRD.

1 Introduction

As the dominant alkaline gas in the atmosphere, NH_3 neutralizes sulfuric and nitric acids to form secondary inorganic aerosol (SIA), thereby exerting a strong but nonlinearly control on $PM_{2.5}$ formation (Behera and Sharma, 2012; Lelieveld et al., 2015). Existing studies suggest that NH_3 reduction can effectively reduce $PM_{2.5}$ pollution (Zhai et al., 2021), with Pearl River Delta (PRD) focused modeling studies showing that NH_3 emission control is efficient for nitrate reduction and can be particularly effective during pollution episodes (Qin et al., 2015; Yin et al., 2018). NH_3 abatement has also been shown to have a lower marginal abatement cost than further reductions of SO_2 and NO_x (Gu et al., 2021; Liu et al., 2023). Recently China tightened its Ambient Air Quality Standards (GB 3095-2026) by lowering the annual mean $PM_{2.5}$ limit for Level-I standards from 15 to 10 μg m^{-3} and for Level-II standards from 35 to 25 μg m^{-3}. The Pearl River Delta region also released the Outline of the Beautiful Guangzhou Plan (2025-2035) explicitly calling for tighter control of NH_3 emissions from agricultural production and livestock breeding. To comply with increasingly stringent air quality standard, strengthening NH_3 control would be an important pathway.

Accurate quantification of the spatiotemporal distribution of NH_3 emissions is a prerequisite for assessing NH_3 impacts on $PM_{2.5}$ formation and design cost-effective $PM_{2.5}$ mitigation pathways. Over the past decades, numerous studies have relied on bottom-up NH_3 emission inventories at global, national, and regional scales (Crippa et al., 2018; Geng et al., 2024; Hoesly et al., 2018; Kang et al., 2016) to examine effectiveness of NH_3 emission control for $PM_{2.5}$ mitigation (Gu et al., 2021; Liu et al., 2019; Tang et al., 2025). However, current bottom-up NH_3 inventories for China show substantial variability across different studies, with annual total emissions for 2015 estimated to range from 9.8 to 20.8 Tg yr^{-1} (Chen et al., 2023). This spread indicates substantial uncertainties in current bottom-up estimates. Agricultural activities dominate anthropogenic NH_3 emissions in China, but their bottom-up estimation remains challenging because activity data and emission factors vary with local meteorology, soil conditions, and management practices (Beusen et al., 2008; Xu et al., 2019; Zhang et al., 2017). Non-agricultural NH_3 sources, including traffic, waste, residential, and industrial sectors, are increasingly recognized as important contributors in urban and densely populated regions (Tang et al., 2025; Wu et al., 2020). Their estimates within existing inventories still remain highly uncertain, arising from diverse emission sources, each requires extensive experimental data characterizing emission factors and their dependence, which remain largely insufficient in

https://doi.org/10.5194/egusphere-2026-4773
Preprint. Discussion started: 8 September 2026

many existing inventories (Sutton et al., 2000; Van Damme et al., 2018; Yan et al., 2024).

Model-observation comparisons have revealed substantial discrepancies in simulated NH_3, NH_4^+, and nitrogen deposition when using existing NH_3 inventories, e.g., 42.5%-76.3% underestimation in simulated NH_3 columns relative to satellite retrievals (Li et al., 2021) and 5%-60% underestimation in simulated wet NH_4^+ deposition over hotspot regions in China (Tan et al., 2022). With observations available, top-down inverse modeling could identify systematic biases in prior emission inventories and derive posterior emission estimates that are statistically optimal given assumed prior and observational error structure. Previous inversion work for China's NH_3 emissions generally suggest that inventories underestimate NH_3 emissions (Chen et al., 2025; Jin et al., 2023; Kong et al., 2019). Top-down estimates of China's total NH_3 emissions during 2016-2018 ranged from 15.4 to 17.5 Tg yr^{-1}, whereas bottom-up estimates ranged only from 10.4 to 11.6 Tg yr^{-1} (Liu et al., 2025).

Guangdong is a representative humid subtropical province where urban-industrial NH_3 sources in the PRD coexist with dispersed agricultural sources in surrounding non-PRD areas. Its frequent summertime precipitation and hot, humid climate largely challenges the validity of traditional NH_3 emission factor parameterization in emission inventories. A previous study showed that simulated atmospheric NH_3 have large biases with surface measurements owing to underestimation of traffic emission sources in dry season and overestimation of agricultural sources in wet season (Sheng et al., 2025). Isotope-based studies also indicate that non-agricultural NH_3 emissions are likely underestimated in current bottom-up inventories (Chen et al., 2022; Jiang et al., 2022). These limitations reduce the reliability of current NH_3 inventories for environmental assessment and policy formulation, cultivating the need for setting up more observations that help constrain and correct emission inventories. Therefore, improving NH_3 emission estimates for Guangdong requires not only an inversion but also a sector-resolved framework that can separately constrain agricultural and non-agricultural sources.

However, dense ground-based NH_3 observations remain scarce because NH_3 is both difficult and expensive to measure. Previous inverse analyses have used NH_4^+ wet deposition (Paulot et al., 2014), surface NH_3 concentrations (Kong et al., 2019), and satellite NH_3 column density (Cao et al., 2020; Marais et al., 2021; Zhu et al., 2013) as observational constraints. But nationwide observation network (e.g., for NH_4^+ wet deposition, surface NH_3) and satellite products used in previous research remain spatially too sparse to resolve emission patterns at provincial scales. The Acid Deposition Monitoring Network in East Asia (EANET) provides NH_4^+ wet deposition but includes only 7 sites in China (Paulot et al., 2014). The Ammonia Monitoring Network in China (AMoN-China) provides surface NH_3 observations for 53 sites across the entire China (Kong et al., 2019). By contrast, satellite instruments such as Infrared Atmospheric Sounding Interferometer (IASI) provide broad spatial coverage, but their retrievals can exhibit substantial and highly variable uncertainties and suffer from extensive data gaps under cloudy conditions (Ge et al., 2020; Van Damme et al., 2015; Van Damme et al., 2017). As a result, only few research has inversely estimated NH_3 emissions for agricultural

https://doi.org/10.5194/egusphere-2026-4773
Preprint. Discussion started: 8 September 2026

and non-agricultural sources separately for major Chinese regions (Tang et al., 2025; Xu et al., 2023).

Here we develop an inversion framework to provide monthly improved NH_3 emission estimates for agricultural and non-agricultural sectors in Guangdong Province in 2023. We take advantage of a ground-based NH_3 observation network consisting of 9 sites and the recently available FY-4B satellite NH_3 column observations with denser temporal coverage and cloud-free sampling than IASI (He et al., 2025; Yang et al., 2025; Zeng et al., 2023), to improve a localized 3 km × 3 km NH_3 emission inventory characterizing high spatiotemporal heterogeneity for Guangdong (Huang et al., 2021) through GEOS-Chem High Performance simulation in stretched grids allowing for at ~0.1° × 0.1° resolution over Guangdong. Bayesian algorithm is used for inverse modeling. National Nitrogen Deposition Monitoring Network (NNDMN) data is used for independent validation of posterior inventory. Our findings help constrain agricultural and non-agricultural NH_3 emission estimations, their seasonality, and could improve assessments of $PM_{2.5}$ control effectiveness of addressing NH_3 from various sources. This framework can be applied to other regions where agricultural and urban NH_3 sources coexist under complex meteorological conditions.

2 Methods

2.1 Observational constraints for NH_3 inversion

We used NH_3 total column observations from the Chinese Fengyun-4B (FY-4B) geostationary satellite, corrected with ground based NH_3 observations from Pearl River Delta (PRD) monitoring network (Huang et al., 2024) to constrain NH_3 emissions in both PRD and the surrounding non-PRD region within Guangdong Province. FY-4B, launched in 2021, carries the Geostationary Interferometric Infrared Sounder (GIIRS), a hyperspectral thermal infrared sounder that provides repeated observations over East Asia with high temporal sampling (Yang et al., 2025). Compared with low-Earth-orbit infrared sounders such as IASI, FY-4B provides much denser temporal coverage over the same location (Sheng et al., 2026). This is useful for capturing diurnal NH_3 variability, increasing cloud-free sampling opportunities, and improving constraints over low-latitude regions such as southern China (He et al., 2025; Zeng et al., 2023). Retrievals of NH_3 based on the optimal estimation method have been evaluated in detail and show a high degree of consistency with IASI, CrIS, and ground-based observations (Sheng et al., 2026). These advantages make FY-4B particularly suitable for regional NH_3 emission inversion in Guangdong. Hourly NH_3 measurements from the PRD ground-based monitoring network were used to correct the FY-4B-derived surface NH_3 concentrations. After data-availability screening and quality control, observations from nine ground-based sites across eight PRD cities in 2023 were retained for this study (Figure S1 and Table S1). Previous applications have demonstrated the value of this NH_3 monitoring network for evaluating NH_3 distributions and diagnosing biases in regional NH_3 emission inventories (Sheng et al., 2025).

https://doi.org/10.5194/egusphere-2026-4773
Preprint. Discussion started: 8 September 2026

In this study, 2-hourly FY-4B NH_3 retrievals were first quality-controlled by removing negative values and then regridded to 0.2° × 0.2° resolution. Monthly means NH_3 columns were subsequently converted to surface NH_3 concentrations using model-derived column-to-surface conversion factors, which account for the vertical distribution of NH_3 modeled by GEOS-Chem High Performance (GCHP) model. Specifically, GCHP outputs on the cubed-sphere grid were first regridded to 0.2° × 0.2° to match the FY-4B grid. Modeled NH_3 columns (unit: molec cm^{-2}) were obtained by vertically integrating the layered NH_3 fields, while the NH_3 concentration in the lowest model layer was used as a proxy for surface NH_3 concentration (unit: μg m^{-3}). The modeled ratio of surface concentration to total column was then applied to the FY-4B NH_3 columns to derive FY-4B-based surface NH_3 concentrations:

$$C_{\mathrm{surf,FY,i}} = \Omega_{\mathrm{FY,i}} \times \left(\frac{C_{\mathrm{surf,GCHP,i}}}{\Omega_{\mathrm{GCHP,i}}}\right) \quad (1)$$

where $\Omega_{\mathrm{FY,i}}$ is the FY-4B NH_3 column at grid i, $C_{\mathrm{surf,GCHP,i}}$ is the lowest-layer GCHP NH_3 concentration at the same grid, and $\Omega_{\mathrm{GCHP,i}}$ is the vertically integrated GCHP NH_3 column.

The satellite-converted surface NH_3 concentrations were further corrected using ground-based NH_3 observations, which provide direct in situ constraints on near-surface NH_3 and were used as reference measurements for bias correction. Specifically, we applied a multiplicative bias correction approach combined with inverse distance weighting (IDW) interpolation to correct the FY-4B-derived surface NH_3 field using monthly mean ground-based observations (Lotrecchiano et al., 2023). At each monitoring site, a station-specific correction factor was calculated as the ratio of the ground-observed NH_3 concentration to the corresponding FY-4B-derivedsurface NH_3 concentration. These correction factors were then spatially interpolated across the FY-4B grid using IDW and used to scale the original FY-4B-derived surface NH_3 field, yielding the corrected surface NH_3 concentrations:

$$C_{\mathrm{surf,FY,i}}^{fused} = C_{\mathrm{surf,FY,i}} \times \frac{\sum_{j=1}^{N}\left(\frac{1}{d_{ij}^{p}} \times \frac{y_j}{C_{\mathrm{surf,FY,j}}}\right)}{\sum_{j=1}^{N}\left(\frac{1}{d_{ij}^{p}}\right)} \quad (2)$$

where $C_{\mathrm{surf,FY,i}}$ is the FY-4B NH_3 concentrations at grid i, y_j is the ground observation at station j, $C_{\mathrm{surf,FY,j}}$ is the FY-4B NH_3 concentrations at station j, dij is the distance from grid i to station j, $p = 2$ is the IDW power parameter.

This procedure generated a monthly surface NH_3 concentration field that combines the broad

https://doi.org/10.5194/egusphere-2026-4773
Preprint. Discussion started: 8 September 2026

spatial coverage of geostationary satellite observations and the near-surface fidelity of in situ measurements. This fused field was then used as the observational constraint in the Bayesian inversion.

2.2 Nitrogen deposition data for independent validation of inversion

We used nitrogen deposition observations from two sites within National Nitrogen Deposition Monitoring Network (NNDMN) (Wen et al., 2024) to evaluate GCHP simulation results with prior and posterior NH_3 emission estimates. The two sites are Guangzhou Baiyun (23.16 °N, 113.27 °E) and Zhanjiang (21.26 °N, 110.33 °E) and we utilized 2023 measurements of NH_3 concentration, NH_4^+ concentration, and dry and wet deposition rates for independent validation. NNDMN is a long-term nationwide monitoring network in China and have been widely used for NH_3 inversion (Chen et al., 2025).

2.3 Prior emission inventory for Guangdong

We used a localized high-resolution emission inventory (Guangdong Emission Inventory; GD-EI) for GCHP simulation, and its source-resolved NH_3 emissions as the prior for inversion, compared with coarser inventories, GD-EI combines a finer source-classification framework with localized activity data, updated emission factors, and source-specific spatial allocation methods, including farmland-productivity proxies for agricultural sources and point-source allocation for major industrial sources (Huang et al., 2021). This model-ready provincial inventory provides gridded emissions at 3 km × 3 km resolution for nine major atmospheric pollutants, including SO_2, NO_x, CO, VOCs, BC, OC, NH_3, $PM_{2.5}$, and PM_{10}. The updated version we used incorporates more localized activity data, updated emission factors, and improved spatial and temporal allocation methods for most pollutant emission estimation, compared with its earlier development (Bian et al., 2019; Zhong et al., 2018) or national inventory. It thus would reduce emission estimation uncertainties and better represent intra-provincial emission heterogeneity in Guangdong. For NH_3, these improvements help better reproduce the spatial distribution characteristics of agricultural and non-agricultural emissions in Guangdong, providing a credible spatial and sectoral basis for the subsequent region- and sector-specific inversion. Because the latest available GD-EI dataset was for 2022, we used GD-EI (2022) as the prior for the 2023 inversion. In our inversion framework, the prior mainly provides initial spatial pattern and sectoral partition of NH_3 emissions, whereas the monthly regional emission amount would be optimized through scaling factors calculated by inverse model.

Given small budgets of individual nonagricultural NH_3 sectors and similar spatial distribution, in inversion, we have decided to obtain statistically optimized monthly NH_3 emission scaling factors for agricultural (including livestock and fertilizer application) and aggregated nonagricultural sectors (including power generation, stationary combustion, transportation,

https://doi.org/10.5194/egusphere-2026-4773
Preprint. Discussion started: 8 September 2026

dust, solvent use, storage, biomass burning, industrial processes, and other anthropogenic sources). According to GD-EI, anthropogenic NH_3 emissions over Guangdong totaled 477.6 kt yr^{-1}, of which 437.2 kt yr^{-1} arose from agricultural sources and 40.4 kt yr^{-1} from non-agricultural sources (power: 2.9 kt, combustion: 1.1 kt, transportation: 8.1 kt, biomass: 1.8 kt, process: 0.9 kt and other sources: 25.7 kt). Spatially, emissions were concentrated mainly outside the PRD, while the PRD exhibited a relatively larger share of non-agricultural NH_3 emissions (14.4%) than the non-PRD region (6.2%). This grouping preserves the main contrast between agricultural and non-agricultural NH_3 emissions and keeps the inversion problem low-dimensional. The prior spatial distributions of NH_3 emissions from individual GD-EI source categories are shown in Figure S4.

2.4 GCHP model settings

We adopted the GEOS-Chem High Performance model (GCHP, v14.6.3) for air quality simulation at ~0.1° × 0.1° over Guangdong and simulated NH_3 concentration fields are used for inverse modeling. The stretched-grid capability of GCHP allows high-resolution simulations over a user-defined target region while retaining global coverage (Eastham et al., 2018; Ye et al., 2024). This configuration is particularly suitable as it enables fine-resolution simulation over Guangdong without the need for externally prescribed lateral boundary conditions required by conventional nested-grid simulations, thereby avoiding additional uncertainties associated with boundary-condition specification (Nesser et al., 2025).

The Jacobian matrix required for inversion, representative of the sensitivity of NH_3 concentrations to regional-sectoral NH_3 emissions, are obtained through perturbation experiments (Table 1). As shown in Table 1, there is one baseline simulation (BASE) and eight emission perturbation simulations (increase or decrease NH_3 emission from agricultural and non-agricultural sectors, respectively, by 50% in PRD and non-PRD region), all other settings than NH_3 emissions are the same. This perturbation-based, finite-difference approach is commonly used in emission inversion studies, including NH_3 inversions (Li et al., 2019; Li et al., 2025). The ±50% perturbation was selected to provide a detectable model response while remaining within the range of emission changes commonly examined in NH_3 sensitivity studies (Kim et al., 2021; Liu et al., 2021). We acknowledge that aerosol responses to NH_3 emission changes are nonlinear; therefore, the Jacobian matrix is treated as a local linear approximation around the prior emissions. The validity of this approximation was further evaluated by comparing the linearly reconstructed posterior NH_3 concentrations with an independent posterior GCHP simulation (Text S3).

Table 1 GCHP simulations included in this study. Simulation cases and NH_3 sectoral emission perturbation ratios compared to BASE are shown. Abbreviations: AGR (agricultural); NAGR (non-agricultural); non-PRD (NPRD).

Simulation cases	NH_3 emission perturbation ratio (region & sector)

	PRD region		Non-PRD region	
	Agricultural	**Non-agricultural**	**Agricultural**	**Non-agricultural**
BASE	0%	0%	0%	0%
PRD_AGR_+50	+50%	0%	0%	0%
PRD_AGR_-50	-50%	0%	0%	0%
PRD_NAGR_+50	0%	+50%	0%	0%
PRD_NAGR_-50	0%	-50%	0%	0%
NPRD_AGR_+50	0%	0%	+50%	0%
NPRD_AGR_-50	0%	0%	-50%	0%
NPRD_NAGR_+50	0%	0%	0%	+50%
NPRD_NAGR_-50	0%	0%	0%	-50%

To assess how much the optimized emissions improve agreement with the observations, we performed an additional GCHP simulation driven by the posterior emissions derived from the Bayesian inversion (posterior simulation). The agreement of the prior and posterior simulations with the fused FY-4B-ground surface NH_3 concentration field was evaluated using the normalized mean bias (NMB) and normalized root mean square error (NRMSE), with the detailed calculation methods provided in Text S2. In addition to this NH_3-based evaluation, we also used independent observations to examine whether GCHP reasonably reproduced the broader chemical environment relevant to NH_3-NH_4^+ partitioning and secondary inorganic aerosol formation. Hourly $PM_{2.5}$ and O_3 observations from the China National Environmental Monitoring Centre (CNEMC; https://air.cnemc.cn:18007/) network over Guangdong, together with hourly particulate NH_4^+, SO_4^{2-}, and NO_3^- measurements from the PRD ion-monitoring sites (Huang et al., 2024), were aggregated to monthly means and compared with GCHP outputs sampled at the corresponding monitoring locations. The CNEMC observations were used to evaluate the model performance for major air pollutants, while the PRD ion measurements were used to assess the representation of particulate ammonium, sulfate, and nitrate that influence NH_3 gas-particle partitioning. These datasets were used only for model evaluation and were not assimilated in the inversion.

2.5 Bayesian inversion algorithm

We adopted the traditional basic Bayesian "big region approach" (Chen et al., 2025; Stavrakou and J., 2006) to optimize NH_3 emissions and quantify posterior uncertainties. In this framework, Guangdong Province was divided into the PRD and non-PRD regions. Anthropogenic NH_3 emissions were grouped into two sectors, agricultural and non-agricultural, and separate inversions were performed for the PRD and non-PRD regions. For each month m and region r, the inversion optimizes only two sectoral scaling factors ($f_{m,r,Agri}$ and $f_{m,r,NonAgri}$), corresponding to agricultural and non-agricultural NH_3 emissions. The corresponding state vector $\mathbf{x}_{m,r}$ is defined as:

https://doi.org/10.5194/egusphere-2026-4773
Preprint. Discussion started: 8 September 2026

$$\mathbf{x}_{m,r} = \begin{bmatrix} f_{m,r,\mathrm{Agri}} \\ f_{m,r,\mathrm{NonAgri}} \end{bmatrix} \tag{3}$$

where each element of $\mathbf{x}_{m,r}$ is dimensionless. The prior state $\mathbf{x}_{a,m,r} = [1\ 1]^{\mathrm{T}}$. Posterior emissions are obtained by scaling the prior emissions in each region–sector group:

$$\widehat{\boldsymbol{E}_{m,r}} = \mathbf{x}_{m,r} \odot \boldsymbol{E}_{a,m,r} \tag{4}$$

where $\odot$ denotes element-wise multiplication over the two sector groups, and $\mathbf{E}_{a,m,r}$ represents the prior sectoral emissions vector for region r and month m.

The Jacobian matrix $\mathbf{K}_{m,r}$ represents the local sensitivity of NH_3 concentration to changes in emission scaling factors in $\mathbf{x}_{m,r}$. We approximate the model response as linear in the vicinity of the prior emissions. For each month and region, one emission group was perturbed at a time by −50% and +50% relative to the baseline simulation (0%), while all other groups were kept fixed. The sensitivities in $\mathbf{K}_{m,r}$ were then estimated by linear regression using the three perturbation simulations.

Assuming Gaussian errors with diagonal prior and observational covariance matrices, $\mathbf{S}_{a,m,r}$ and $\mathbf{S}_{o,m,r}$, the posterior scaling factors have the analytic solution:

$$\hat{\mathbf{x}}_{m,r} = \mathbf{x}_{a,m,r} + \left(\mathbf{K}_{m,r}^{T}\mathbf{S}_{o,m,r}^{-1}\mathbf{K}_{m,r} + \mathbf{S}_{a,m,r}^{-1}\right)^{-1}\mathbf{K}_{m,r}^{T}\mathbf{S}_{o,m,r}^{-1}\left(\mathbf{y}_{m,r} - \mathbf{K}_{m,r}\mathbf{x}_{a,m,r}\right) \tag{5}$$

where $\mathbf{y}_{m,r}$ denotes the observational vector used for region r and month m.

And the posterior covariance is:

$$\widehat{\mathbf{S}_{m,r}} = \left(\mathbf{K}_{m,r}^{T}\mathbf{S}_{o,m,r}^{-1}\mathbf{K}_{m,r} + \mathbf{S}_{a,m,r}^{-1}\right)^{-1} \tag{6}$$

The diagonal elements of $\widehat{\mathbf{S}_{m,r}}$ provide the posterior variances of the optimized scaling factors. The deviation uncertainty for each posterior scaling factor was calculated as the square root of the corresponding diagonal element of $\widehat{\mathbf{S}_{m,r}}$, and was converted to emission uncertainty by multiplying by the corresponding prior monthly emissions. These uncertainties are shown as error bars in Figure 4.

We assume diagonal prior and observation error covariance matrices ($S_{a,m,r}$ and $S_{o,m,r}$) for each month m and region r, consistent with the big-region Bayesian framework. We set the prior uncertainty of the agricultural NH_3 emission to 100% (Zhang et al., 2018). For the non-agricultural group, we adopt a larger prior uncertainty of 300% to reflect the substantially higher

https://doi.org/10.5194/egusphere-2026-4773
Preprint. Discussion started: 8 September 2026

uncertainties associated with combustion and industry related NH_3 emissions and their emission factors (Meng et al., 2017; Zheng et al., 2012).

For observational errors, we assume spatially uncorrelated errors and therefore use a diagonal $S_{o,m,r}$. S_O is populated using the residual error method (Heald et al., 2004; Liang et al., 2024), where observational error variances are derived from the residual mismatch between observations and prior simulations after removal of the mean bias.

2.6 Sectoral NH_3 emission removal sensitivity experiments in GCHP and $PM_{2.5}$ health benefits assessment

With our inversed NH_3 emission inventory, we further evaluate contribution of agricultural and non-agricultural NH_3 emission to $PM_{2.5}$ air pollution formation in Guangdong province. We conducted two additional hypothetical experiments in GCHP, where agricultural and non-agricultural NH_3 emissions were removed by 100%, respectively (abbreviated as AGR NH_3 emission removal and NAGR NH_3 emission removal scenarios). $PM_{2.5}$ reductions were calculated as the difference between the posterior simulation and each sensitivity experiment scenario. Avoided premature deaths attributable to reduced long-term $PM_{2.5}$ exposure were estimated using the Global Exposure Mortality Model, (Burnett et al., 2018) following the procedures described in Text S4.

3 Results

3.1 Evaluation of prior and posterior NH_3 simulations

Our posterior NH_3 emission inventory improves GCHP-simulated spatial distribution and magnitude of surface NH_3 concentrations over Guangdong relative to the prior inventory. Figure 1 shows our observation constraint, i.e., surface NH_3 concentrations converted from FY-4B column data after corrections with ground-based measurement, and a comparison to GCHP-simulated surface NH_3 concentrations with both prior and posterior NH_3 emission inventory. Our posterior simulation better captures the observed spatial variability of surface NH_3 than the prior simulation. The posterior simulation shifts a substantial fraction of data points toward the 1:1 line, particularly in the low-to-moderate concentration range where most observations are distributed (Figure.1c). The posterior simulation substantially reduces the overall model bias, with the magnitude of NMB decreasing by 48.9% compared with the prior simulation, from 9.0% to 4.6%. Meanwhile, NRMSE decreases by 12.5%, from 55.3% to 48.4%, indicating an overall improvement in model-observation agreement. The reductions in the absolute values of NMB and NRMSE indicate that the posterior simulation is overall closer to observations, suggesting that the inversion effectively reduced the simulation bias and improved representation of surface NH_3 concentrations.

https://doi.org/10.5194/egusphere-2026-4773
Preprint. Discussion started: 8 September 2026

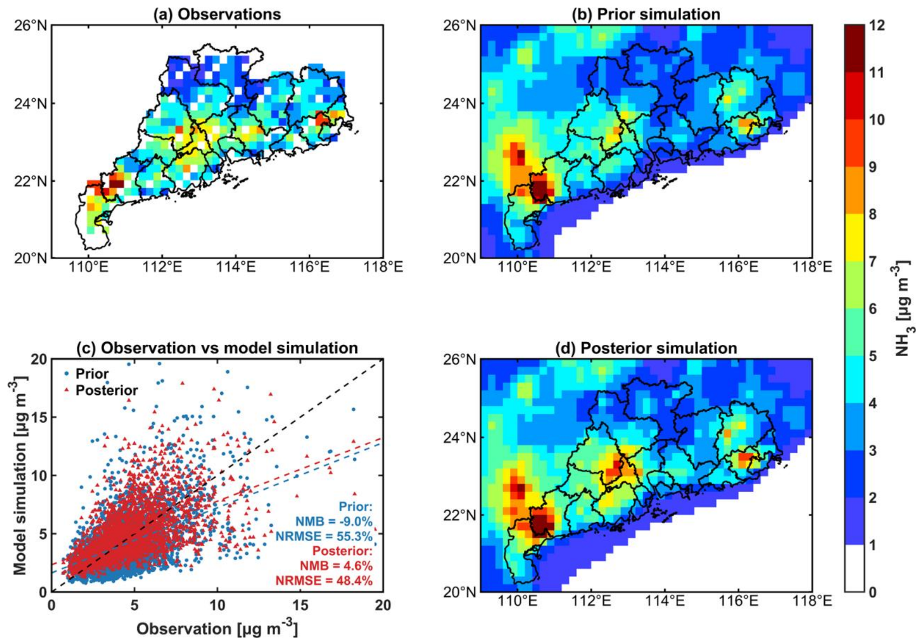

Figure 1. Comparison of observation-constrained and GCHP-simulated surface NH_3 concentrations over Guangdong. (a) Spatial distribution of surface NH_3 concentrations over Guangdong converted from FY-4B column using GCHP vertical profiles and corrected by 9 sites of ground-based observations, GCHP simulations using the prior (b) and posterior (d) NH_3 emission inventories, (c) evaluation of simulated NH_3 concentrations in b and d against observations in a.

Independent evaluation against two NNDMN sites shows that the posterior inventory improves reduced nitrogen simulation, particularly NH_3 concentrations and NH_x dry deposition, whereas improvements for particulate NH_4^+ and wet NH_4^+ deposition simulation are moderate (Figure 2). Compared with the prior simulation, the posterior simulated NH_3 concentrations (NH_x dry deposition) are much closer to measurements and substantially reduce NMB from -34.6% to -5.8% (from -49% to -25%) (Figure 2a and c). Improvements in simulated NH_4^+ are small (Figure 2b), with a relatively large residual NRMSE. This is likely owing to issues with model representation for other processes such as gas-particle partitioning, transport, and deposition. The remaining bias in wet NH_4^+ deposition is also consistent with the residual bias in simulated NH_4^+ concentration and may be further affected by uncertainties in model representation of precipitation, wet scavenging, and cloud processes (Figure 2d). Overall, the independent evaluation shows that the posterior inventory improves model performance across multiple NH_3 related metrics, while also indicating that model uncertainties in NH_3-NH_4^+ partitioning and wet removal processes cannot be fully resolved by optimizing NH_3 emissions alone.

https://doi.org/10.5194/egusphere-2026-4773
Preprint. Discussion started: 8 September 2026

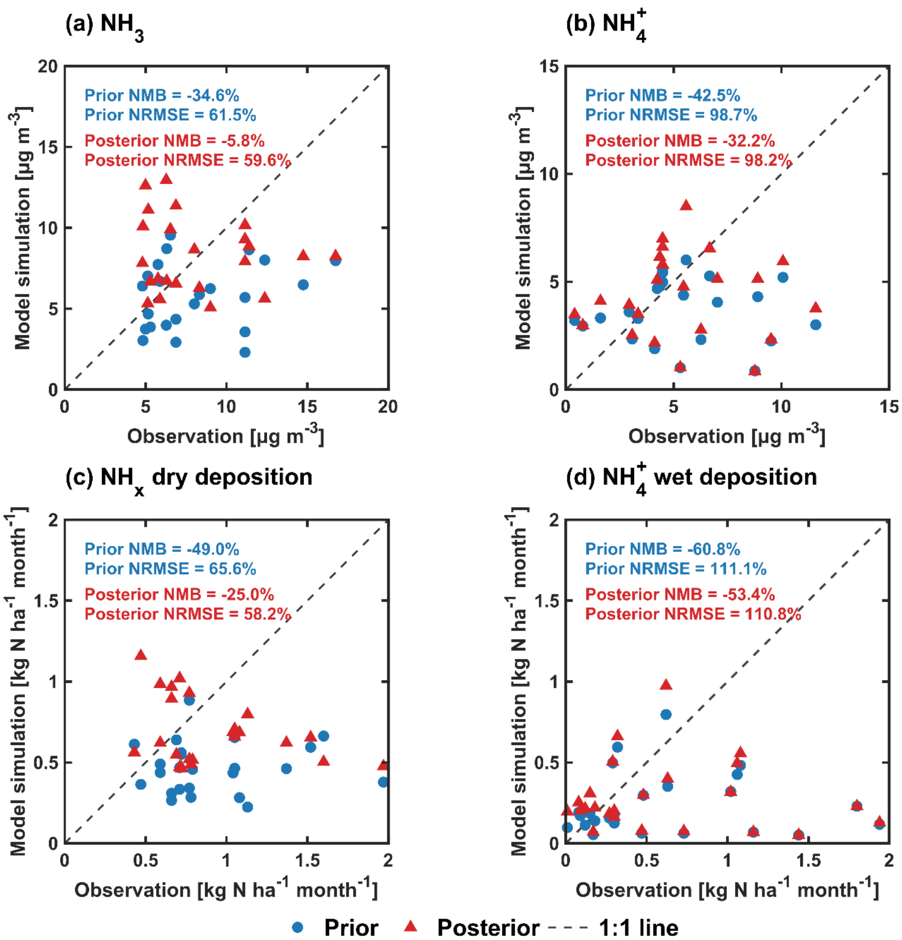

419

https://doi.org/10.5194/egusphere-2026-4773
Preprint. Discussion started: 8 September 2026

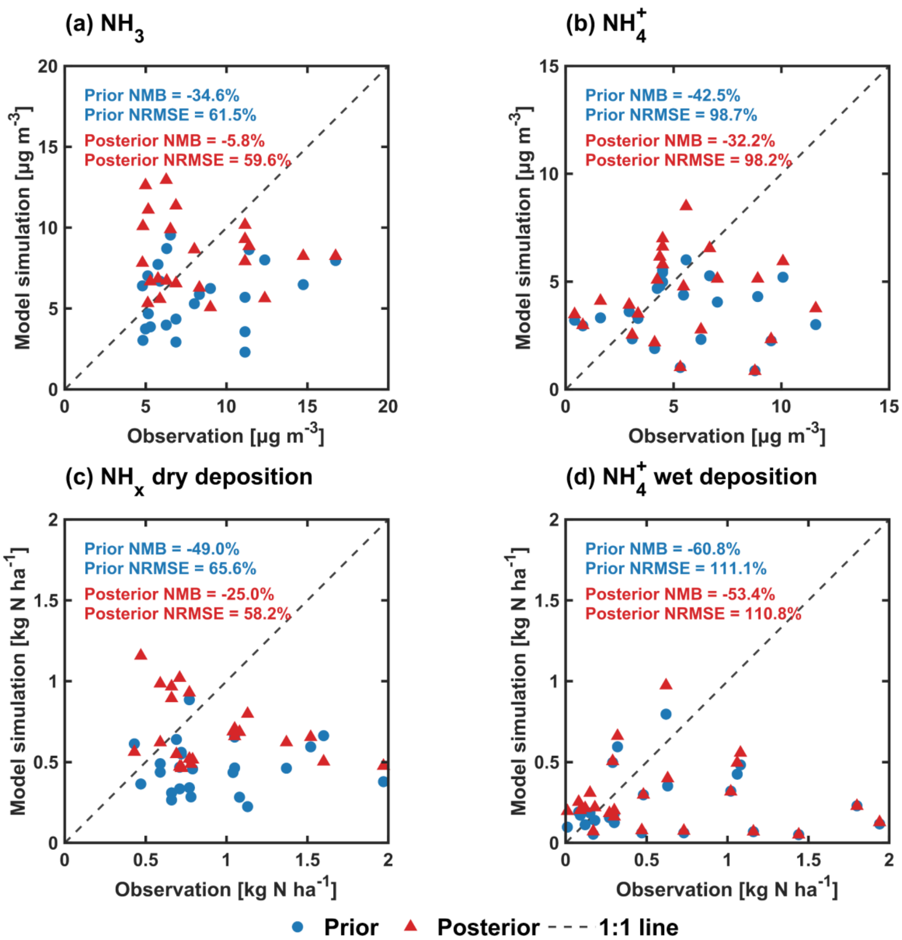

Figure 2. Independent validation of prior and posterior NH_3 emission inventory through comparing GCHP simulated monthly NH_3 and NH_4^+ concentrations and nitrogen deposition with two observation sites from the NNDMN network. (a) NH_3 concentrations, simulation using prior NH_3 emission inventory denoted by blue dots and using posterior inventory denoted by red triangles. (b) NH_4^+ concentrations, (c) dry deposition fluxes of NH_x ($NH_3 + NH_4^+$), and (d) wet deposition fluxes of NH_4^+.

3.2 Posterior NH_3 emission inventory and monthly variability

Our inversed inventory for Guangdong, compared to the prior, modestly reduces annual total NH_3 emission estimates by 7.6%, decreases agricultural emission estimates by 17.1% and increases nonagricultural emission estimates by 95.5%. Our inversion provides contrasting sectoral adjustments: agricultural emissions reduced from 437.2 to 362.5 kt, whereas non-agricultural emissions increased from 40.4 to 79.0kt, and emission totals decrease from 477.6 to 441.5 kt. These contrasting sectoral adjustments indicate that the prior inventory likely

https://doi.org/10.5194/egusphere-2026-4773
Preprint. Discussion started: 8 September 2026

overestimates agricultural NH_3 emissions while underestimating non-agricultural sources at the provincial scale.

Spatially our inversion would increase NH_3 emission intensity in localized urban PRD and several connected urban corridors, but decrease in diffused rural agricultural areas that are mostly in non-PRD region (Figure 3). Regionally, agricultural emissions decrease by 4.0% in the PRD and by 21.6% in the non-PRD, whereas non-agricultural emissions increase by 101.9% in the PRD and by 89.7% in the non-PRD. This spatial pattern suggests that the prior inventory likely overallocated emissions to broad agricultural regions while underrepresenting urban non-agricultural NH_3 sources. This interpretation is consistent with recent isotope-based source apportionment evidence showing that non-agricultural NH_3 emissions in China are substantially underestimated in bottom-up inventories, with particularly large corrections in major urban agglomerations such as the PRD (Yan et al., 2024), and with PRD-specific inventory diagnosis showing overestimated agricultural emissions, particularly during the wet period, and underestimated non-agricultural sources (Sheng et al., 2025). Potentially missing or weakly constrained urban sources include vehicle exhaust from gasoline three-way catalysts and diesel selective catalytic reduction systems, NH_3 slip from power and industrial NO_x-control systems, waste treatment and residential activities (Chen et al., 2022; Wen et al., 2023). Because many of these sources are associated with localized industrial facilities, built-up areas, and road traffic, their emissions may be poorly represented in inventories that rely on unlocalized emission factors, incomplete source coverage, or simplified spatial allocation proxies, thereby contributing to the underrepresentation of urban NH_3 hotspots.

https://doi.org/10.5194/egusphere-2026-4773
Preprint. Discussion started: 8 September 2026

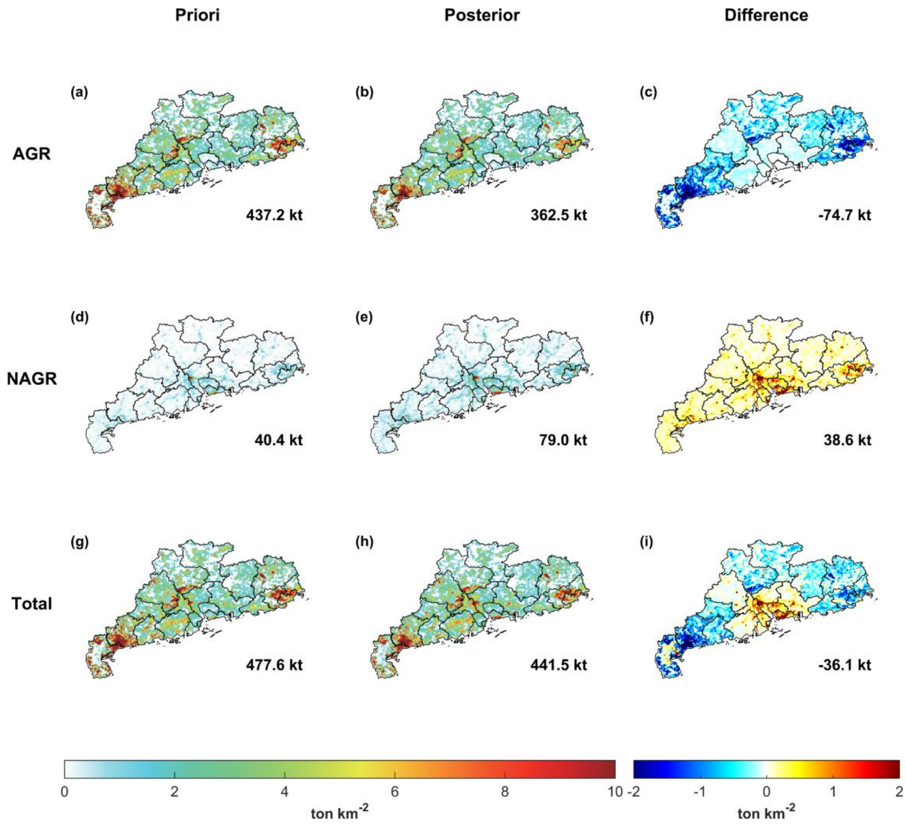

Figure 3. Spatial distribution of prior and posterior annual agricultural, nonagricultural and total NH_3 emissions in Guangdong Province in 2023. The 1st, 2nd and 3rd column represent prior emissions, posterior emissions, and posterior-minus-prior differences, respectively. 1st, 2nd and 3rd rows represent agricultural (a, b, c), non-agricultural (d, e, f), and total emissions (g, h, i).

Monthly scale factors reveal a pronounced seasonal redistribution of NH_3 emissions in both the PRD and non-PRD regions, with opposite seasonal adjustments for agricultural and non-agricultural sources (Figure 4). In both regions, agricultural emissions were generally reduced during most warm-season months, especially where the prior inventory exhibited the strongest summer maxima, whereas the reductions became weaker and, in some cases, reversed during cooler months. This pattern suggests that the prior inventory likely overestimates the warm-season agricultural peak but underrepresents cool-season agricultural emissions. In contrast, non-agricultural emissions were enhanced in nearly all months in both the PRD and non-PRD regions, with the largest scale factors occurring in the cool season and smaller adjustments during the warm season. These monthly adjustments indicate that the prior inventory underestimates non-agricultural NH_3 emissions throughout the year, particularly during cooler months.

https://doi.org/10.5194/egusphere-2026-4773
Preprint. Discussion started: 8 September 2026

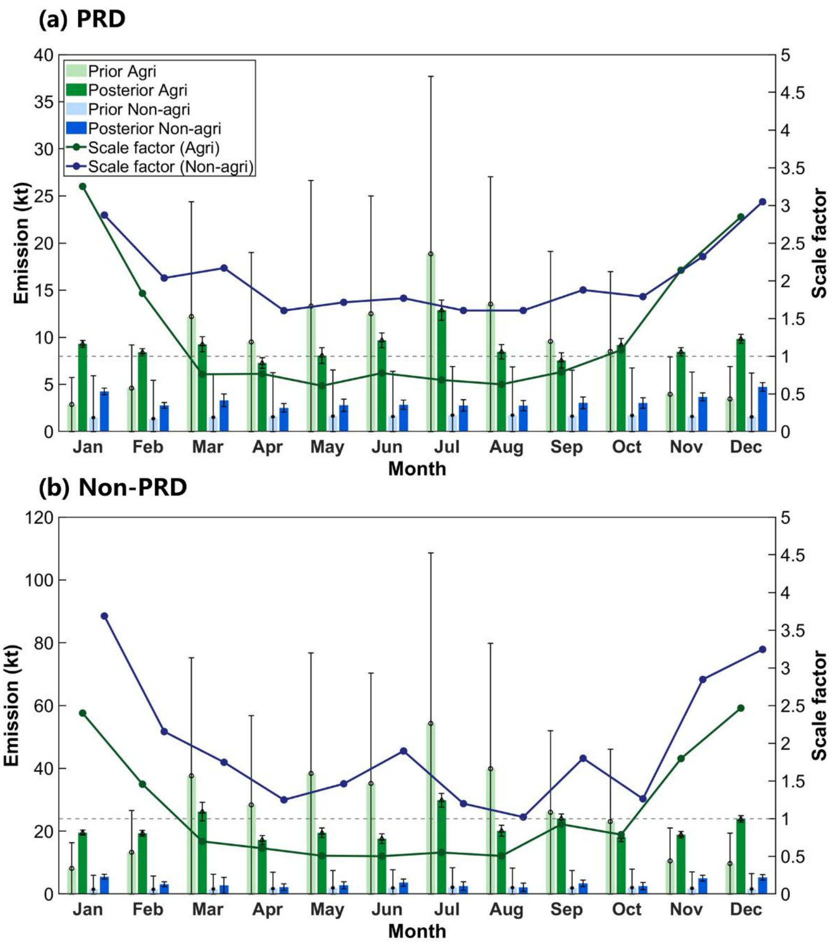

Figure 4. Monthly scale factors (posterior/prior) for agricultural and non-agricultural NH_3 emissions in PRD and non-PRD regions of Guangdong Province in 2023. Bars show monthly NH_3 emissions on the left y-axis, with light and dark colors representing prior and posterior emissions, respectively. Green and blue indicate agricultural and non-agricultural emissions, respectively. Lines with markers show posterior-to-prior scaling factors on the right y-axis. Error bars indicate uncertainties of prior and posterior emission, calculated from the assumed prior covariance matrix and the posterior covariance matrix, respectively. Panels show (a) PRD (b) non-PRD regions.

3.3 Air quality and health benefits from hypothetical agricultural v.s. non-agricultural NH_3 emission reductions

Sectoral NH_3 emission removal experiments in GCHP using posterior inventory reveal distinct air quality and health implications of agricultural and non-agricultural NH_3 emissions in

https://doi.org/10.5194/egusphere-2026-4773
Preprint. Discussion started: 8 September 2026

Guangdong, reflecting differences in both emission magnitude and population exposure. Figure 5 shows $PM_{2.5}$ reductions from two sectoral NH_3 emission removal scenarios and associated premature death reductions. For its large share in total NH_3 emissions (82.1%), zeroing out agricultural sources produce a much larger reduction in regional $PM_{2.5}$ concentrations (3.74 μg m^{-3} averaged for Guangdong) and more lives saved (3251 persons) than removing non-agricultural NH_3 emissions (0.72 μg m^{-3} and 1064 persons). The area fraction of Guangdong with annual mean $PM_{2.5}$ below 25 μg m^{-3} (Level-II standards) increases from 54.8% in the posterior simulation to 84.3% under agricultural NH_3 removal, but only to 58.8% under non-agricultural NH_3 removal. Largest local $PM_{2.5}$ reductions can be up to 6.7 μg m^{-3} in northwestern Guangdong near Zhaoqing and 4.8 μg m^{-3} in surrounding areas outside of Guangdong under the AGR NH_3 removal scenario. In contrast, $PM_{2.5}$ reductions under the NAGR NH_3 removal scenario are mainly confined to the PRD and are smaller, with the largest local reduction of only 3.1 μg m^{-3} over Guangzhou.

Premature death reductions occurred for PRD and non-PRD regions are quite balanced (1622 and 1629 persons, respectively), if removing agricultural NH_3 emissions in Guangdong. As most agricultural emissions are located in non-PRD region, health benefits in PRD likely come from high population number, high baseline $PM_{2.5}$ exposure (35.4 μg m^{-3}, compared to 23.5 μg m^{-3} in non-PRD) and reduced regional air pollution from controlling surrounding agricultural NH_3 sources. Fig. 5c indicates there exist three major clusters that enjoy $PM_{2.5}$ reduction health benefits, i.e. the central PRD, eastern Guangdong coastal cities, and parts of western Guangdong. In contrast, removing nonagricultural NH_3 emissions which mostly locate in PRD provide localized health benefits (821 reduced deaths in PRD), which is more substantial than regional benefits (243 reduced deaths in non-PRD).

https://doi.org/10.5194/egusphere-2026-4773
Preprint. Discussion started: 8 September 2026

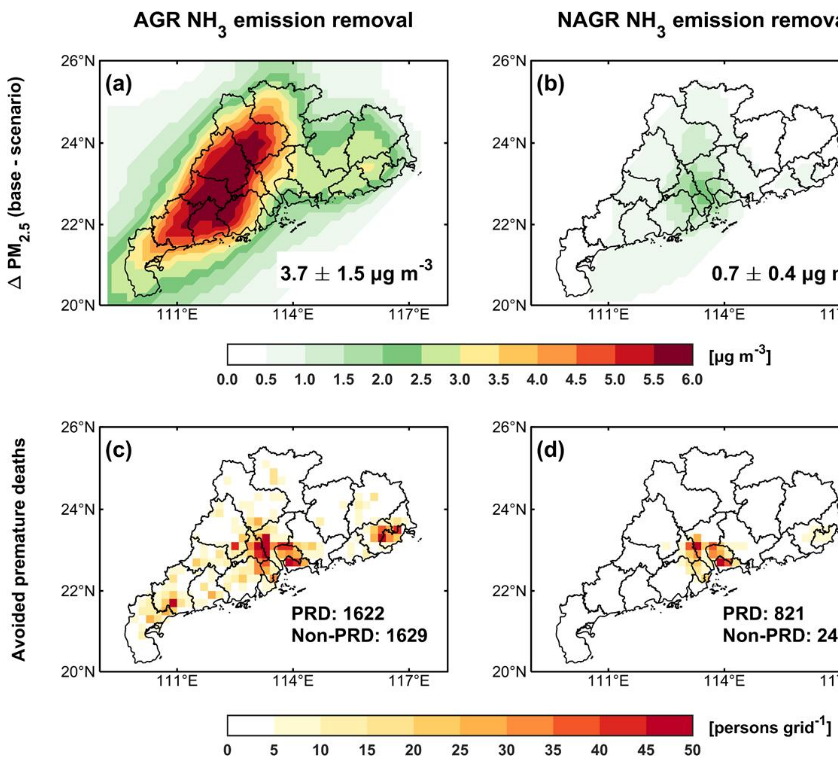

Figure 5. $PM_{2.5}$ reductions and avoided premature deaths under hypothetical agricultural and non-agricultural NH_3 emission removal scenarios. Panels (a) and (b) show annual mean $PM_{2.5}$ reductions calculated as the posterior simulation minus the corresponding sensitivity experiment scenario for agricultural and non-agricultural NH_3 emissions, respectively. Panels (c) and (d) show the associated avoided premature deaths relative to the posterior simulation. The values annotated in panels (a) and (b) represent the mean ± spatial standard deviation across valid grid cells. The values annotated in panels (c) and (d) represent total avoided premature deaths summed over the PRD and non-PRD regions. Positive values indicate reductions relative to the posterior simulation.

4 Conclusion and Discussion

This study developed a Bayesian inversion framework by integrating ground-based NH_3 measurements, FY-4B geostationary retrievals, a 3 km × 3 km local inventory, and stretched-grid GCHP simulations. Compared with most previous NH_3 emission inversion work that optimized emissions at the national scale over China (Chen et al., 2025; Jin et al., 2023; Kong et al., 2019) or Beijing-Hebei-Tianjin region (Xu et al., 2023), eastern China (Tang et al., 2025), we provide monthly scale factors for agricultural and non-agricultural NH_3 emissions in PRD and rest of Guangdong, respectively, which is a humid subtropical region with a mixture of agricultural and urban emission sources that are not that well studied and air quality

https://doi.org/10.5194/egusphere-2026-4773
Preprint. Discussion started: 8 September 2026

implications of improved sectoral NH_3 emission estimates are examined using two hypothetical sensitivity experiments in GCHP. Our posterior emission estimates moderately reduced provincial annual NH_3 emissions from 477.6 to 441.5 kt yr^{-1}, in which agricultural emissions decreased from 437.2 to 362.5 kt yr^{-1}, while non-agricultural emissions increased from 40.4 to 79.0 kt yr^{-1}. Regionally, agricultural emissions decrease by 4.0% in PRD and 21.6% in non-PRD, whereas non-agricultural emissions increase by 101.9% and 89.7%, respectively. Thus, the prior inventory overestimated warm-season agricultural emissions while underrepresented urban non-agricultural sources, especially during the cool season. Posterior simulations showed improved agreement with corrected FY-4B and ground-based observations, and reasonably good independent evaluation with two NNDMN site measurements. Removing agricultural NH_3 emissions reduces annual mean $PM_{2.5}$ by 3.7 μg m^{-3} and avoids 3251 premature deaths, compared with 0.7 μg m^{-3} and 1064 avoided deaths for non-agricultural NH_3 removal, indicating that agricultural NH_3 control remains important for reducing the province-wide $PM_{2.5}$ burden and supporting progress toward the stricter $PM_{2.5}$ targets under GB 3095-2026. However, because non-agricultural NH_3 sources overlap more strongly with densely populated areas, especially in the PRD, non-agricultural NH_3 controls in those areas can provide substantial public-health benefits despite their smaller emission mass.

The NH_3 inventory adopted in this study is of higher geographical resolution and adopted more complicated categorization for agricultural sources (Huang et al., 2021), we collected other national or regional NH_3 emission inventories and compare their estimates for Guangdong with our prior and posterior (Figure S19). Our inversion mainly corrects the seasonal allocation of the prior inventory, i.e., shift NH_3 emissions a bit more from warm season to cool season. The prior inventory exhibits a much sharper summer peak and lower winter emissions than most available inventories, whereas the posterior emission shifts part of the emissions from the warm season to the cool season and produces a flatter annual cycle within the range of published estimates. This seasonal redistribution is qualitatively consistent with recent observation-constrained studies, which point to underestimated non-agricultural emissions and uncertain agricultural temporal allocation in existing inventories (Chen et al., 2022; Li et al., 2021; Sheng et al., 2025).

Previous studies in the PRD have emphasized the important role of NH_3 in secondary inorganic aerosol formation and $PM_{2.5}$ mitigation, particularly through its influence on particulate ammonium and nitrate under different chemical regimes and emission-control scenarios (Qin et al., 2015; Wang et al., 2016; Yin et al., 2018). Building on this context, our study extends current understanding of how $PM_{2.5}$ responds to NH_3 emission reductions in Guangdong by conducting sector-specific sensitivity experiments with an observation-constrained posterior NH_3 inventory. The posterior inventory and sensitivity experiments together show that removing agricultural NH_3 produces a larger province-wide $PM_{2.5}$ response than removing non-agricultural NH_3, mainly because agricultural sources account for the majority of total NH_3 emissions. Agricultural NH_3 removal also substantially increases the area of Guangdong with annual mean $PM_{2.5}$ below the 25 μg m^{-3} threshold, suggesting that agricultural NH_3 mitigation

https://doi.org/10.5194/egusphere-2026-4773
Preprint. Discussion started: 8 September 2026

is important for meeting concentration-based air quality targets at the provincial scale. However, the health benefits of NH_3 controls are not determined by emission magnitude alone. Although non-agricultural NH_3 accounts for a much smaller fraction of total NH_3 emissions, its removal produces substantial avoided premature deaths in the PRD because non-agricultural NH_3 hotspots are more closely co-located with densely populated urban areas. Therefore, non-agricultural NH_3 controls should not be overlooked in Guangdong, especially in the PRD, where reductions in urban NH_3 sources can provide important public health benefits.

Nevertheless, uncertainties remain in observational constraints, model representation, and inversion design, and these uncertainties may affect the magnitude and seasonal allocation of the posterior NH_3 adjustments. First, our satellite NH_3 column-to-surface conversion depends on GCHP modeled vertical profiles and remains an important uncertainty source, although FY-4B provides valuable geostationary sampling over Guangdong and the correction using ground-based observations reduces part of the uncertainty associated with converting satellite columns to near-surface NH_3 concentrations. More sophisticated approaches could explicitly account for satellite vertical sensitivity by applying retrieval averaging kernels and replacing priori profiles with spatially and temporally resolved model-simulated NH_3 vertical profiles (Clarisse et al., 2023; Liu et al., 2025). In this study, we adopted a surface-to-column conversion followed by ground-based correction because our inversion was designed to combine FY-4B observations and near-surface NH_3 constraint, in which surface observations help correct part of the uncertainty introduced during the column-to-surface conversion. Second, model uncertainties may also influence the posterior estimates. Biases in acid precursor emissions, sulfate and nitrate formation, deposition, and aerosol thermodynamics can affect simulated NH_3-NH_4^+ partitioning and therefore the emission adjustments inferred by the inversion. For example, overestimated acidic precursor concentrations could enhance the conversion of gaseous NH_3 to particulate NH_4^+, leading the inversion to compensate by adjusting NH_3 emissions (Chen et al., 2025). Although our evaluation against China National Environmental Monitoring Centre (CNEMC) observations and PRD ion measurements helps reduce this concern (Text S2), uncertainties in acid gas emissions and aerosol processes may still propagate into posterior NH_3 emission estimates. Third, the limited number of nitrogen deposition sites restricts the use of deposition observations as inversion constraints. In this study, deposition measurements from NNDMN were reserved for independent evaluation because only two sites were available in Guangdong. Expanding ground-based NH_3, particulate NH_4^+, and deposition monitoring would allow future inversions to incorporate these observations as additional constraints rather than relying on NH_3 alone.

In addition, the regional-sectoral scaling design keeps the inversion tractable under current observational constraints, but it also limits the degree of spatial and source-specific detail that can be independently inferred. Therefore, future work aiming to better distinguish individual non-agricultural sources would require denser and more source-informative observational constraints, especially in urban areas where these sources are mixed. Expanding ground monitoring across traffic corridors, waste-management areas, residential districts, and industrial

https://doi.org/10.5194/egusphere-2026-4773
Preprint. Discussion started: 8 September 2026

zones, would help future inversions move from broad non-agricultural scaling toward more detailed subsector-level optimization.

Overall, our NH_3 emission inversion for Guangdong suggested that current inventory needs to better represent the seasonal allocation of agricultural emissions and the magnitude and spatial distribution of non-agricultural NH_3 sources. With improved NH_3 emissions, our unveiled $PM_{2.5}$ response indicate that reducing agricultural NH_3 emissions remains important for province-wide $PM_{2.5}$ mitigation, while reductions in non-agricultural NH_3 emissions can also provide meaningful health benefits in densely populated urban agglomerations such as the PRD. These findings provide a basis for improving NH_3 emission inventories and for designing more targeted NH_3 control strategies that support continued air quality improvement and public health protection in Guangdong.

Supporting information:

Description of GCHP model configuration, ground-based measurements, model evaluation metrics, Bayesian cost function, and $PM_{2.5}$-related premature mortality calculation. Additional figures showing observation networks, FY-4B NH_3 observations, corrected surface NH_3 fields, sectoral GD-EI emissions, model evaluations, meteorological comparisons, monthly prior and posterior NH_3 emission distributions, population distribution, and comparison with other NH_3 inventories. Tables listing PRD observation sites and bottom-up inventory details

Acknowledgements:

This study was supported by the National Science Foundation of China (Grant No. 42505174, 42230602, T2522032) and HKUST (GZ) start-up funds.

Competing interests:

The contact author has declared that none of the authors has any competing interests.

Data availability:

The Guangdong Emission Inventory, NH_3 observations from Pearl River Delta (PRD) monitoring network, FY-4B NH_3 satellite retrievals and nitrogen deposition observations from the National Nitrogen Deposition Monitoring Network (NNDMN) will be made available on request. The population data is available from the LandScan website (https://landscan.ornl.gov/). The GEOS-Chem High Performance (v14.6.3) are available from the International GEOS-Chem User Community (https://zenodo.org/records/16541830).

Author contributions:

Y.G. conceived the idea. L.M. and N.L. conducted the research with equal contribution. Z.Z., Z.C., Z.M., T.Z., D.C., X.L., J.Z., Y.Z., and L.Z. contributed data and analytical tools. L.Z., Y.Z., L.M., N.L., and Y.G. designed the model experiments. L.M. performed the experiments, inversion and processed the data. L.M., Y.G., and N.L. analyzed the data and designed the visualization. L.M., Y.G., and N.L. wrote the original draft, incorporating constructive advice from all authors.

References

Behera, S. N., and Sharma, M.: Transformation of atmospheric ammonia and acid gases into components of PM2.5: an environmental chamber study, Environ. Sci. Pollut. Res., 19, 1187-1197, https://doi.org/10.1007/s11356-011-0635-9, 2012.

Beusen, A. H. W., Bouwman, A. F., Heuberger, P. S. C., Van Drecht, G., and Van Der Hoek, K. W.: Bottom-up uncertainty estimates of global ammonia emissions from global agricultural production systems, Atmos. Environ., 42, 6067-6077, https://doi.org/https://doi.org/10.1016/j.atmosenv.2008.03.044, 2008.

Bian, Y., Huang, Z., Ou, J., Zhong, Z., Xu, Y., Zhang, Z., Xiao, X., Ye, X., Wu, Y., Yin, X., Li, C., Chen, L., Shao, M., and Zheng, J.: Evolution of anthropogenic air pollutant emissions in Guangdong Province, China, from 2006 to 2015, Atmos. Chem. Phys., 19, 11701-11719, https://doi.org/10.5194/acp-19-11701-2019, 2019.

Burnett, R., Chen, H., Szyszkowicz, M., Fann, N., Hubbell, B., Pope, C. A., Apte, J. S., Brauer, M., Cohen, A., Weichenthal, S., Coggins, J., Di, Q., Brunekreef, B., Frostad, J., Lim, S. S., Kan, H., Walker, K. D., Thurston, G. D., Hayes, R. B., Lim, C. C., Turner, M. C., Jerrett, M., Krewski, D., Gapstur, S. M., Diver, W. R., Ostro, B., Goldberg, D., Crouse, D. L., Martin, R. V., Peters, P., Pinault, L., Tjepkema, M., van Donkelaar, A., Villeneuve, P. J., Miller, A. B., Yin, P., Zhou, M., Wang, L., Janssen, N. A. H., Marra, M., Atkinson, R. W., Tsang, H., Quoc Thach, T., Cannon, J. B., Allen, R. T., Hart, J. E., Laden, F., Cesaroni, G., Forastiere, F., Weinmayr, G., Jaensch, A., Nagel, G., Concin, H., and Spadaro, J. V.: Global estimates of mortality associated with long-term exposure to outdoor fine particulate matter, Proceedings of the National Academy of Sciences, 115, 9592-9597, https://doi.org/10.1073/pnas.1803222115, 2018.

Cao, H., Henze, D. K., Shephard, M. W., Dammers, E., Cady-Pereira, K., Alvarado, M., Lonsdale, C., Luo, G., Yu, F., Zhu, L., Danielson, C. G., and Edgerton, E. S.: Inverse modeling of NH_3 sources using CrIS remote sensing measurements, Environ. Res. Lett., 15, 104082, https://doi.org/10.1088/1748-9326/abb5cc, 2020.

Chen, J., Cheng, M., Krol, M., de Vries, W., Zhu, Q., Liu, X., Zhang, F., and Xu, W.: Trends in anthropogenic ammonia emissions in China since 1980: A review of approaches and estimations, Front. Environ. Sci., 11, 1133753, https://doi.org/10.3389/fenvs.2023.1133753, 2023.

Chen, J., Du, X., Liu, X., Xu, W., and Krol, M.: Estimation of Ammonia Emissions over China Using IASI Satellite-Derived Surface Observations, Environ. Sci. Technol., 59, 9991-10000, https://doi.org/10.1021/acs.est.4c10878, 2025.

Chen, Y., Zhang, Q., Cai, X., Zhang, H., Lin, H., Zheng, C., Guo, Z., Hu, S., Chen, L., Tao, S., Liu, M., and Wang, X.: Rapid Increase in China's Industrial Ammonia Emissions: Evidence from Unit-Based Mapping, Environ. Sci. Technol., 56, 3375-3385, https://doi.org/10.1021/acs.est.1c08369, 2022.

Chen, Z., Pei, C., Liu, J., Zhang, X., Ding, P., Dang, L., Zong, Z., Jiang, F., Wu, L., Sun, X., Zhou, S., Zhang, Y., Zhang, Z., Zheng, J., Tian, C., Li, J., and Zhang, G.: Non-agricultural source dominates the ammonium aerosol in the largest city of South China based on the vertical δ15N measurements, Sci. Total Environ., 848, 157750, https://doi.org/https://doi.org/10.1016/j.scitotenv.2022.157750,

https://doi.org/10.5194/egusphere-2026-4773
Preprint. Discussion started: 8 September 2026

2022.

Clarisse, L., Franco, B., Van Damme, M., Di Gioacchino, T., Hadji-Lazaro, J., Whitburn, S., Noppen, L., Hurtmans, D., Clerbaux, C., and Coheur, P.: The IASI NH3 version 4 product: averaging kernels and improved consistency, Atmos. Meas. Tech., 16, 5009-5028, https://doi.org/10.5194/amt-16-5009-2023, 2023.

Crippa, M., Guizzardi, D., Muntean, M., Schaaf, E., Dentener, F., van Aardenne, J. A., Monni, S., Doering, U., Olivier, J. G. J., Pagliari, V., and Janssens-Maenhout, G.: Gridded emissions of air pollutants for the period 1970–2012 within EDGAR v4.3.2, Earth Syst. Sci. Data, 10, 1987-2013, https://doi.org/10.5194/essd-10-1987-2018, 2018.

Eastham, S. D., Long, M. S., Keller, C. A., Lundgren, E., Yantosca, R. M., Zhuang, J., Li, C., Lee, C. J., Yannetti, M., Auer, B. M., Clune, T. L., Kouatchou, J., Putman, W. M., Thompson, M. A., Trayanov, A. L., Molod, A. M., Martin, R. V., and Jacob, D. J.: GEOS-Chem High Performance (GCHP v11-02c): a next-generation implementation of the GEOS-Chem chemical transport model for massively parallel applications, Geosci. Model Dev., 11, 2941-2953, https://doi.org/10.5194/gmd-11-2941-2018, 2018.

Ge, X., Schaap, M., Kranenburg, R., Segers, A., Reinds, G. J., Kros, H., and de Vries, W.: Modeling atmospheric ammonia using agricultural emissions with improved spatial variability and temporal dynamics, Atmos. Chem. Phys., 20, 16055-16087, https://doi.org/10.5194/acp-20-16055-2020, 2020.

Geng, G., Liu, Y., Liu, Y., Liu, S., Cheng, J., Yan, L., Wu, N., Hu, H., Tong, D., Zheng, B., Yin, Z., He, K., and Zhang, Q.: Efficacy of China's clean air actions to tackle PM2.5 pollution between 2013 and 2020, Nat. Geosci., 17, 987-994, https://doi.org/10.1038/s41561-024-01540-z, 2024.

Gu, B., Zhang, L., Van Dingenen, R., Vieno, M., Van Grinsven, H. J., Zhang, X., Zhang, S., Chen, Y., Wang, S., Ren, C., Rao, S., Holland, M., Winiwarter, W., Chen, D., Xu, J., and Sutton, M. A.: Abating ammonia is more cost-effective than nitrogen oxides for mitigating $PM_{2.5}$ air pollution, Science, 374, 758-762, https://doi.org/10.1126/science.abf8623, 2021.

He, T., Oomen, G., Tang, W., Bouarar, I., Chance, K., Clerbaux, C., Edwards, D. P., Eskes, H., Gaubert, B., Granier, C., Guevara, M., Jacob, D. J., Kaiser, J., Kim, J., Kondragunta, S., Liu, X., Marais, E. A., Miyazaki, K., Park, R., Peuch, V., Pfister, G., Richter, A., Stavrakou, T., Suleiman, R. M., Turner, A. J., Veihelmann, B., Zeng, Z., and Brasseur, G. P.: Challenges and Opportunities Offered by Geostationary Space Observations for Air Quality Research and Emission Monitoring, Bull. Amer. Meteorol. Soc., 106, E939-E963, https://doi.org/https://doi.org/10.1175/BAMS-D-23-0145.1, 2025.

He, Y., Ding, X., He, Q., Zhang, Y., Chen, D., Zhang, T., Yang, K., Wang, J., Cheng, Q., Jiang, H., Wang, Z., Liu, P., Wang, X., and Boy, M.: Long-term Trends in $PM_{2.5}$ Chemical Composition and Its Impact on Aerosol Properties: Field Observations from 2007 to 2020 in Pearl River Delta, South China, Atmos. Chem. Phys., 25, 13729-13745, https://doi.org/10.5194/acp-25-13729-2025, 2025.

Heald, C. L., Jacob, D. J., Jones, D. B. A., Palmer, P. I., Logan, J. A., Streets, D. G., Sachse, G. W., Gille, J. C., Hoffman, R. N., and Nehrkorn, T.: Comparative inverse analysis of satellite (MOPITT) and aircraft (TRACE-P) observations to estimate Asian sources of carbon monoxide, Journal of Geophysical Research: Atmospheres, 109, https://doi.org/https://doi.org/10.1029/2004JD005185, 2004.

Hoesly, R. M., Smith, S. J., Feng, L., Klimont, Z., Janssens-Maenhout, G., Pitkanen, T., Seibert, J. J., Vu, L., Andres, R. J., Bolt, R. M., Bond, T. C., Dawidowski, L., Kholod, N., Kurokawa, J., Li, M.,

https://doi.org/10.5194/egusphere-2026-4773
Preprint. Discussion started: 8 September 2026

Liu, L., Lu, Z., Moura, M. C. P., O'Rourke, P. R., and Zhang, Q.: Historical (1750–2014) anthropogenic emissions of reactive gases and aerosols from the Community Emissions Data System (CEDS), Geosci. Model Dev., 11, 369-408, https://doi.org/10.5194/gmd-11-369-2018, 2018.

Huang, G., Xiao, L., Chen, Z., Zhang, T., Zhong, Z., Fang, X., Liao, T., and Chen, D.: Study on atmospheric ammonia distribution and contribution to PM2.5 in typical areas of Pearl River Delta, China Environmental Science, 09, 4796-4804, https://doi.org/10.19674/j.cnki.issn1000-6923.20240412.010, 2024.

Huang, Z., Zhong, Z., Sha, Q., Xu, Y., Zhang, Z., Wu, L., Wang, Y., Zhang, L., Cui, X., Tang, M., Shi, B., Zheng, C., Li, Z., Hu, M., Bi, L., Zheng, J., and Yan, M.: An updated model-ready emission inventory for Guangdong Province by incorporating big data and mapping onto multiple chemical mechanisms, Sci. Total Environ., 769, 144535, https://doi.org/https://doi.org/10.1016/j.scitotenv.2020.144535, 2021.

Jiang, M., Zhang, Z., Li, T., Lin, B., Zhang, Z., Liao, T., Yuan, L., Pan, S., Li, J., and Zhang, G.: Source Apportionment of Ammonium in Atmospheric PM2.5 in the Pearl River Delta Based on Nitrogen Isotope, Ecology and Environment, 31, 1840-1848, https://doi.org/10.16258/j.cnki.1674-5906.2022.09.014, 2022.

Jin, J., Fang, L., Li, B., Liao, H., Wang, Y., Han, W., Li, K., Pang, M., Wu, X., and Xiang Lin, H.: 4DEnVar-based inversion system for ammonia emission estimation in China through assimilating IASI ammonia retrievals, Environ. Res. Lett., 18, 34005, https://doi.org/10.1088/1748-9326/acb835, 2023.

Kang, Y., Liu, M., Song, Y., Huang, X., Yao, H., Cai, X., Zhang, H., Kang, L., Liu, X., Yan, X., He, H., Zhang, Q., Shao, M., and Zhu, T.: High-resolution ammonia emissions inventories in China from 1980 to 2012, Atmos. Chem. Phys., 16, 2043-2058, https://doi.org/10.5194/acp-16-2043-2016, 2016.

Kim, E., Kim, B., Kim, H. C., and Kim, S.: Sensitivity of fine particulate matter concentrations in South Korea to regional ammonia emissions in Northeast Asia, Environ. Pollut., 273, 116428, https://doi.org/https://doi.org/10.1016/j.envpol.2021.116428, 2021.

Kong, L., Tang, X., Zhu, J., Wang, Z., Pan, Y., Wu, H., Wu, L., Wu, Q., He, Y., Tian, S., Xie, Y., Liu, Z., Sui, W., Han, L., and Carmichael, G.: Improved Inversion of Monthly Ammonia Emissions in China Based on the Chinese Ammonia Monitoring Network and Ensemble Kalman Filter, Environ. Sci. Technol., 53, 12529-12538, https://doi.org/10.1021/acs.est.9b02701, 2019.

Lelieveld, J., Evans, J. S., Fnais, M., Giannadaki, D., and Pozzer, A.: The contribution of outdoor air pollution sources to premature mortality on a global scale, Nature, 525, 367-371, https://doi.org/10.1038/nature15371, 2015.

Li, B., Chen, L., Shen, W., Jin, J., Wang, T., Wang, P., Yang, Y., and Liao, H.: Improved gridded ammonia emission inventory in China, Atmos. Chem. Phys., 21, 15883-15900, https://doi.org/10.5194/acp-21-15883-2021, 2021.

Li, C., Martin, R. V., Shephard, M. W., Cady-Pereira, K., Cooper, M. J., Kaiser, J., Lee, C. J., Zhang, L., and Henze, D. K.: Assessing the Iterative Finite Difference Mass Balance and 4D-Var Methods to Derive Ammonia Emissions Over North America Using Synthetic Observations, Journal of Geophysical Research: Atmospheres, 124, 4222-4236, https://doi.org/https://doi.org/10.1029/2018JD030183, 2019.

Li, S., Dammers, E., Segers, A., and Erisman, J. W.: Local-scale inversion of agricultural ammonia emissions: a case study on Schiermonnikoog, the Netherlands, Atmos. Chem. Phys., 25, 15593-15611, https://doi.org/10.5194/acp-25-15593-2025, 2025.

Liang, R., Zhang, Y., Hu, Q., Li, T., Li, S., Yuan, W., Xu, J., Zhao, Y., Zhang, P., Chen, W., Zhuang, M., Shen, G., and Chen, Z.: Satellite-Based Monitoring of Methane Emissions from China's Rice Hub, Environ. Sci. Technol., 58, 23127-23137, https://doi.org/10.1021/acs.est.4c09822, 2024.

Liu, M., Huang, X., Song, Y., Tang, J., Cao, J., Zhang, X., Zhang, Q., Wang, S., Xu, T., Kang, L., Cai, X., Zhang, H., Yang, F., Wang, H., Yu, J. Z., Lau, A. K. H., He, L., Huang, X., Duan, L., Ding, A., Xue, L., Gao, J., Liu, B., and Zhu, T.: Ammonia emission control in China would mitigate haze pollution and nitrogen deposition, but worsen acid rain, Proc. Natl. Acad. Sci. U. S. A., 116, 7760-7765, https://doi.org/10.1073/pnas.1814880116, 2019.

Liu, Q., Chen, Y., Xu, P., Shen, H., Mai, Z., Zhang, R., Guo, P., Zheng, Z., Luan, T., and Tao, S.: Vertical Profile Corrections Explain Satellite–Inventory Ammonia Discrepancies and Reveal Concentrated Agricultural Sources in China, Environ. Sci. Technol., 59, 21609-21621, https://doi.org/10.1021/acs.est.5c08278, 2025.

Liu, Z., Rieder, H. E., Schmidt, C., Mayer, M., Guo, Y., Winiwarter, W., and Zhang, L.: Optimal reactive nitrogen control pathways identified for cost-effective PM2.5 mitigation in Europe, Nat. Commun., 14, 4246, https://doi.org/10.1038/s41467-023-39900-9, 2023.

Liu, Z., Zhou, M., Chen, Y., Chen, D., Pan, Y., Song, T., Ji, D., Chen, Q., and Zhang, L.: The nonlinear response of fine particulate matter pollution to ammonia emission reductions in North China, Environ. Res. Lett., 16, 34014, https://doi.org/10.1088/1748-9326/abdf86, 2021.

Lotrecchiano, N., Barletta, D., Poletto, M., and Sofia, D.: Comparison of spatial interpolation techniques for innovative air quality monitoring systems, Results Eng., 17, 100937, https://doi.org/https://doi.org/10.1016/j.rineng.2023.100937, 2023.

Marais, E. A., Pandey, A. K., Van Damme, M., Clarisse, L., Coheur, P., Shephard, M. W., Cady-Pereira, K. E., Misselbrook, T., Zhu, L., Luo, G., and Yu, F.: UK Ammonia Emissions Estimated With Satellite Observations and GEOS-Chem, J. Geophys. Res.-Atmos., 126, e2021JD035237, https://doi.org/https://doi.org/10.1029/2021JD035237, 2021.

Meng, W., Zhong, Q., Yun, X., Zhu, X., Huang, T., Shen, H., Chen, Y., Chen, H., Zhou, F., Liu, J., Wang, X., Zeng, E. Y., and Tao, S.: Improvement of a Global High-Resolution Ammonia Emission Inventory for Combustion and Industrial Sources with New Data from the Residential and Transportation Sectors, Environ. Sci. Technol., 51, 2821-2829, https://doi.org/10.1021/acs.est.6b03694, 2017.

Nesser, H., Bowman, K. W., Thill, M. D., Varon, D. J., Randles, C. A., Tewari, A., Cardoso-Saldaña, F. J., Reidy, E., Maasakkers, J. D., and Jacob, D. J.: Predicting and correcting the influence of boundary conditions in regional inverse analyses, Geosci. Model Dev., 18, 9279-9291, https://doi.org/10.5194/gmd-18-9279-2025, 2025.

Paulot, F., Jacob, D. J., Pinder, R. W., Bash, J. O., Travis, K., and Henze, D. K.: Ammonia emissions in the United States, European Union, and China derived by high-resolution inversion of ammonium wet deposition data: Interpretation with a new agricultural emissions inventory (MASAGE_NH3), Journal of Geophysical Research: Atmospheres, 119, 4343-4364, https://doi.org/https://doi.org/10.1002/2013JD021130, 2014.

Qin, M., Wang, X., Hu, Y., Huang, X., He, L., Zhong, L., Song, Y., Hu, M., and Zhang, Y.: Formation of particulate sulfate and nitrate over the Pearl River Delta in the fall: Diagnostic analysis using the

https://doi.org/10.5194/egusphere-2026-4773
Preprint. Discussion started: 8 September 2026

Community Multiscale Air Quality model, Atmos. Environ., 112, 81-89, https://doi.org/https://doi.org/10.1016/j.atmosenv.2015.04.027, 2015.

Sheng, L., Guo, Y., Wu, Y., Huang, Z., Yuan, X., Zhu, K., Wu, L., Zhang, J., Wang, Z., Huang, Y., Zhong, Z., Zhang, T., Chen, D., Wang, B., and Zheng, J.: Evaluation and Diagnosis of Regional Ammonia Emission Inventory in the Pearl River Delta Using Multisite NH_3 Observations and Model Simulations, Environ. Sci. Technol., 59, 19318-19329, https://doi.org/10.1021/acs.est.5c01380, 2025.

Sheng, M., Zhou, R., Hua, J., Han, S., Liu, S., Zhang, L., Wang, W., Dang, R., Cao, H., Chen, Z., Gu, Y., Liu, M., Lee, L., Qi, C., Lu, F., Han, C., Shephard, M. W., Guendouz, N., Viatte, C., Clarisse, L., Van Damme, M., Clerbaux, C., and Zeng, Z. C.: Geostationary observations of atmospheric ammonia over East Asia: spatio-temporal variations revealed by three years of FY-4B/GIIRS measurements, Atmos. Chem. Phys., 26, 7803-7826, https://doi.org/10.5194/acp-26-7803-2026, 2026.

Stavrakou, T., and J., F. M.: Grid-based versus big region approach for inverting CO emissions using Measurement of Pollution in the Troposphere (MOPITT) data, Journal of Geophysical Research Atmospheres, 111, 2006.

Sutton, M. A., Dragosits, U., Tang, Y. S., and Fowler, D.: Ammonia emissions from non-agricultural sources in the UK, Atmos. Environ., 34, 855-869, https://doi.org/https://doi.org/10.1016/S1352-2310(99)00362-3, 2000.

Tan, J., Su, H., Itahashi, S., Tao, W., Wang, S., Li, R., Fu, H., Huang, K., Fu, J. S., and Cheng, Y.: Quantifying the wet deposition of reactive nitrogen over China: Synthesis of observations and models, Sci. Total Environ., 851, 158007, https://doi.org/https://doi.org/10.1016/j.scitotenv.2022.158007, 2022.

Tang, K., Zhang, H., Xu, G., Chang, F., Xu, Y., Miao, J., Cui, X., Jin, J., Li, B., Li, K., Liao, H., and Li, N.: Optimizing ammonia emissions for $PM_{2.5}$ mitigation: environmental and health co-benefits in Eastern China, Atmos. Chem. Phys., 25, 14747-14762, https://doi.org/10.5194/acp-25-14747-2025, 2025.

Van Damme, M., Clarisse, L., Dammers, E., Liu, X., Nowak, J. B., Clerbaux, C., Flechard, C. R., Galy-Lacaux, C., Xu, W., Neuman, J. A., Tang, Y. S., Sutton, M. A., Erisman, J. W., and Coheur, P. F.: Towards validation of ammonia (NH_3) measurements from the IASI satellite, Atmos. Meas. Tech., 8, 1575-1591, https://doi.org/10.5194/amt-8-1575-2015, 2015.

Van Damme, M., Clarisse, L., Whitburn, S., Hadji-Lazaro, J., Hurtmans, D., Clerbaux, C., and Coheur, P.: Industrial and agricultural ammonia point sources exposed, Nature, 564, 99-103, https://doi.org/10.1038/s41586-018-0747-1, 2018.

Van Damme, M., Whitburn, S., Clarisse, L., Clerbaux, C., Hurtmans, D., and Coheur, P.: Version 2 of the IASI NH_3 neural network retrieval algorithm: near-real-time and reanalysed datasets, Atmos. Meas. Tech., 10, 4905-4914, https://doi.org/10.5194/amt-10-4905-2017, 2017.

Wang, N., Lyu, X. P., Deng, X. J., Guo, H., Deng, T., Li, Y., Yin, C. Q., Li, F., and Wang, S. Q.: Assessment of regional air quality resulting from emission control in the Pearl River Delta region, southern China, Sci. Total Environ., 573, 1554-1565, https://doi.org/https://doi.org/10.1016/j.scitotenv.2016.09.013, 2016.

Wen, Y., Zhang, S., Wu, Y., and Hao, J.: Vehicular ammonia emissions: an underappreciated emission source in densely populated areas, Atmos. Chem. Phys., 23, 3819-3828, https://doi.org/10.5194/acp-23-3819-2023, 2023.

Wen, Z., Yu, Z., Si, R., Xu, W., Wang, K., Liu, L., Tang, A., Zhang, F., Keith, G., and Liu, X.: Geographical Distribution of Atmospheric Nitrogen Deposition in China and Its Response to Emission Control Policy, Chin. Geogr. Sci., 34, 1017-1031, https://doi.org/10.1007/s11769-024-1471-4, 2024.

Wu, C., Wang, G., Li, J., Li, J., Cao, C., Ge, S., Xie, Y., Chen, J., Liu, S., Du, W., Zhao, Z., and Cao, F.: Non-agricultural sources dominate the atmospheric NH3 in Xi'an, a megacity in the semi-arid region of China, Sci. Total Environ., 722, 137756, https://doi.org/https://doi.org/10.1016/j.scitotenv.2020.137756, 2020.

Xu, J., Lu, M., Guo, Y., Zhang, L., Chen, Y., Liu, Z., Zhou, M., Lin, W., Pu, W., Ma, Z., Song, Y., Pan, Y., Liu, L., and Ji, D.: Summertime Urban Ammonia Emissions May Be Substantially Underestimated in Beijing, China, Environ. Sci. Technol., 57, 13124-13135, https://doi.org/10.1021/acs.est.3c05266, 2023.

Xu, R., Tian, H., Pan, S., Prior, S. A., Feng, Y., Batchelor, W. D., Chen, J., and Yang, J.: Global ammonia emissions from synthetic nitrogen fertilizer applications in agricultural systems: Empirical and process-based estimates and uncertainty, Glob. Change Biol., 25, 314-326, https://doi.org/https://doi.org/10.1111/gcb.14499, 2019.

Yan, F., Chen, W., Wang, X., Jia, S., Mao, J., Cao, J., and Chang, M.: Significant Increase in Ammonia Emissions in China: Considering Nonagricultural Sectors Based on Isotopic Source Apportionment, Environ. Sci. Technol., 58, 2423-2433, https://doi.org/10.1021/acs.est.3c07222, 2024.

Yang, F., Sun, Y., Liu, M., Song, S., Chen, W., Li, Z., and Wang, L.: A new way to obtain the weighted mean temperature (Tm): Using the Geostationary Interferometric Infrared Sounder (GIIRS) equipped on FengYun Satellite, Atmos. Res., 318, 107997, https://doi.org/https://doi.org/10.1016/j.atmosres.2025.107997, 2025.

Ye, X., Zhang, L., Wang, X., Lu, X., Jiang, Z., Lu, N., Li, D., and Xu, J.: Spatial and temporal variations of surface background ozone in China analyzed with the grid-stretching capability of GEOS-Chem High Performance, Sci. Total Environ., 914, 169909, https://doi.org/https://doi.org/10.1016/j.scitotenv.2024.169909, 2024.

Yin, S., Huang, Z., Zheng, J., Huang, X., Chen, D., and Tan, H.: Characteristics of inorganic aerosol formation over ammonia-poor and ammonia-rich areas in the Pearl River Delta region, China, Atmos. Environ., 177, 120-131, https://doi.org/https://doi.org/10.1016/j.atmosenv.2018.01.005, 2018.

Zeng, Z., Lee, L., Qi, C., Clarisse, L., and Van Damme, M.: Optimal estimation retrieval of tropospheric ammonia from the Geostationary Interferometric Infrared Sounder on board FengYun-4B, Atmos. Meas. Tech., 16, 3693-3713, https://doi.org/10.5194/amt-16-3693-2023, 2023.

Zhai, S., Jacob, D. J., Wang, X., Liu, Z., Wen, T., Shah, V., Li, K., Moch, J. M., Bates, K. H., Song, S., Shen, L., Zhang, Y., Luo, G., Yu, F., Sun, Y., Wang, L., Qi, M., Tao, J., Gui, K., Xu, H., Zhang, Q., Zhao, T., Wang, Y., Lee, H. C., Choi, H., and Liao, H.: Control of particulate nitrate air pollution in China, Nat. Geosci., 14, 389-395, https://doi.org/10.1038/s41561-021-00726-z, 2021.

Zhang, L., Chen, Y., Zhao, Y., Henze, D. K., Zhu, L., Song, Y., Paulot, F., Liu, X., Pan, Y., Lin, Y., and Huang, B.: Agricultural ammonia emissions in China: reconciling bottom-up and top-down estimates, Atmos. Chem. Phys., 18, 339-355, https://doi.org/10.5194/acp-18-339-2018, 2018.

Zhang, X., Wu, Y., Liu, X., Reis, S., Jin, J., Dragosits, U., Van Damme, M., Clarisse, L., Whitburn, S., Coheur, P., and Gu, B.: Ammonia Emissions May Be Substantially Underestimated in China, Environ.

https://doi.org/10.5194/egusphere-2026-4773
Preprint. Discussion started: 8 September 2026

Sci. Technol., 51, 12089-12096, https://doi.org/10.1021/acs.est.7b02171, 2017.

Zheng, J. Y., Yin, S. S., Kang, D. W., Che, W. W., and Zhong, L. J.: Development and uncertainty analysis of a high-resolution NH3 emissions inventory and its implications with precipitation over the Pearl River Delta region, China, Atmos. Chem. Phys., 12, 7041-7058, https://doi.org/https://doi.org/10.5194/acp-12-7041-2012, 2012.

Zhong, Z., Zheng, J., Zhu, M., Huang, Z., Zhang, Z., Jia, G., Wang, X., Bian, Y., Wang, Y., and Li, N.: Recent developments of anthropogenic air pollutant emission inventories in Guangdong province, China, Sci. Total Environ., 627, 1080-1092, https://doi.org/https://doi.org/10.1016/j.scitotenv.2018.01.268, 2018.

Zhu, L., Henze, D. K., Cady-Pereira, K. E., Shephard, M. W., Luo, M., Pinder, R. W., Bash, J. O., and Jeong, G. R.: Constraining U.S. ammonia emissions using TES remote sensing observations and the GEOS-Chem adjoint model, J. Geophys. Res.-Atmos., 118, 3355-3368, https://doi.org/https://doi.org/10.1002/jgrd.50166, 2013.